Electrical Engineering
https://doi.org/10.1007/s00202-022-01673-7

ORIGINAL PAPER

Electrical machines in automotive: evaluation of current technologies and future requirements

Mahir Alani[1] · Yasemin Oner[2] · Ahmed Tameemi[3]

Received: 11 November 2021 / Accepted: 17 September 2022
© The Author(s) 2022

Abstract
This paper presents an evaluation of the current technologies and future requirements of electrical machine in automotive. First, a comparative of ten different electrical machines based on the market available electrical vehicles and hybrid electrical vehicles is made. The aim of the comparison is to evaluate the different electrical machine topologies, structure, operation conditions, and performance. The future design requirements of electrical machine in automotive are presented and several state-of-art electrical machine design techniques have been explored and studied by employing them in the compared ten machines. The conclusion of this work shows that permanent magnet topologies have the highest performance among the different electrical machine topologies and have the potential to meet the future requirements. In addition, aggressive cooling methods, i.e., spray, dripping, semi- or fully flooded, are needed to allow electrical machines to operate with the required power density target. Finally, the design to recycle concept shows the potential to be implemented in future electrical machines with little or no sacrifice of the performance.

Keywords Electrical machine · Automotive · Electric vehicle · Electric car

1 Introduction

Since the second coming of electrical vehicles (EVs) by GM EV1 in 1996, the automotive industry has recognized the potential of such technology as a replacement for the conventional internal combustion engine (ICM). Nevertheless, the immaturity of the electrical motor and battery technologies at that time rendered the EV1 to be incomparable to the ICM vehicles in both performance and cost. However, transportation electrification became a necessity rather than an option due to alarming levels of climate change and the consequent legislation. Therefore, the automotive industry has taken partial steps toward clean vehicles by introducing engine electrification and hybrid electrical vehicles (HEVs) to avoid a dramatic change and to allow the development and evolution of the motor and battery technologies.

Looking into the products of EV and HEV from the 1996 inception to the late-2010s, all the know topologies, i.e., DC field rotor (DC), induction machine (IM), switched reluctance (SR) and permanent magnet (PM) have made a presence in automotive [1]. To the author's knowledge, the first topology to leave the race is the SR, beside Holden-ECO, SR has not been used for this application. This is since the main challenges of SR machines are low power density and torque ripple which are both essential requirements for automotive as well as the need for an unconventional converter which rises the total cost of the drive. The IM and DC have also declined, their current presences are only in Tesla and Renault, respectively. The PM has dominated the automotive market having most of the electric motors including the Tesla's latest 2016 models S. The different PM machine topologies including surface-mounted (SPM), interior (IPM), and PM-assisted synchronous reluctance (SynRel-PM) have all been seen in automotive [1]. Despite the heavy presence of PM machines in automotive,

✉ Mahir Alani
mahir.m.j.alani@gmail.com; mahir.al-ani@nottingham.ac.uk

Ahmed Tameemi
Ahmed.altimimy@uoalfarahidi.edu.iq

[1] Research Fellow in the Power Electronics, Machine and Control Group, Department of Electrical and Electronic Engineering, University of Nottingham, University Park, Nottingham NG7 2RD, UK

[2] Yildiz Technical University, Istanbul, Turkey

[3] Department of Communication Technical Engineering, Al-Farahidi University, Baghdad, Iraq

Published online: 14 November 2022

the fact that PM material is needed makes a great challenge. Therefore, reduced PM design techniques have been proposed and used in the latest technology. Other types of permanent magnets, such as ferrite and AlNiCo have also been fairly explored for automotive applications [2].

Therefore, in this paper, ten different electrical machine designs based on machines used in different EVs and HEVs are selected for a comparative study. The study aims to evaluate the different electrical machines topologies, structure, operation conditions and performance. In addition to electromagnetic performance, mechanical and thermal results have been compared. Furthermore, different state-of-art design techniques have been explored and studied by employing them in the compared machines. This study explores the possibility to push the current limits of electrical machines to meet the future automotive targets.

2 Analysis of different types of electrical machines based on market research

Table 1 presents ten vehicles, both hybrid and full electric, which their electric motors have been selected for comparison in this section.

Figure 1 presents the cross section and winding layout of the ten machines. The machines have been selected based on the availability of the information of the machines in the literature [3–15]. The selected machines have DC, IM and PM topologies, PM machines having SPM, IPM and SynRel-PM rotor topologies with mostly NdFeB magnets and one design (based on Chevrolet Volt 2) with ferrite. The analyses are made using ANSYS package.

Honda Accord (HA) and Civic (HC), having a conventional SPM structure with a concentrated winding. Mechanically, the PMs are buried in the rotor core frame in HA, whereas a retaining sleeve is used in the HC. The designs merit techniques are segmented stator teeth with concentrated winding, therefore, automated winding with high impact factor is an advantage [3]. However, the SPM structure consumes high PM quantity, in addition to the complex aforementioned design features, i.e., buried PM and sleeve, that are required for mechanical safety.

2010 Toyota Prius (TP1) is one of the most compared machines in the field of electrical machines, it has been used as a benchmark for automotive design research in many publications [4]. This is due to the success of the vehicle and the widely available information of the motor. The IPM structure offers high torque per magnet volume and, reluctance torque and consequently wide power-speed range [5, 6]. Similarly, the 2014 Toyota Prius (TP2) have an IPM rotor structure with a new magnet set near the rotor surface. The mechanical design of the rotor has complex-shaped gaps to maintain good mechanical performance and allow for rotor cooling channels.

The Chevrolet Volt two motors (C1) and (C2) having different rotors and the same stator, however, the axial length is smaller in CV2. Both motors are SynRel-PM, CV1 designed with a conservative quantity of NdFeB, whereas, CV2 is one of a very few automotive motors with ferrite. The design utilizes the low cost and mass density of ferrite by employing large arc-shape quantities [7–9].

BMW i3 (BI) and Nissan Leaf (NL) are both EVs in the compared machines in this study. Both motors are SynRel-PM structure with reduced PM quantity. BI with slitting design techniques focusing on utilizing the reluctance torque for the benefit of low magnetic quantity [10, 11]. NL having an unorthodox rotor design with a thicker magnet near the outer rotor radius and V-shaped thinner magnets near the inner radius [12, 13].

Finally, the non-PM machines of Renault Zoe (RZ) and Tesla Model S (TS), having a traditional DC rotor (field wound, FW) and IM structure, respectively [12, 13]. RZ rotor consists of a conventional commutated field winding rotor, it is worth noting that the entire Renault fleet of HEVs and EVs are DC rotor machines [14]. TS IM has tackled the rotor heating issue with a complex but innovative rotor cooling [15].

Table 2 lists the main design parameters of the ten machines. The packing factor of all concentrated winding (CW) and distributed winding (DW) are assumed to be 0.4 and 0.6, respectively. Table 3 presents a summary of the open circuit and electromagnetic load results of the ten machines.

Similar torque density is observed in the PM topologies which is around twice of the non-PM topologies. Power density has a similar trend with the PM topologies having around 3 to 4 times the value of non-PM topologies. Standing out is the CV2 the topology with ferrite, this is due to the large quantity of the low mass density ferrite and the multi-flux paths to allow more reluctance torque.

Torque and power per magnet weight are factors used to estimate the cost of the machine. Beside the SPM topologies which have the best utilization of the PM material, SynRel topologies have overall higher torque and power per magnet weight compared to the IPM. Moreover, utilizing the inverter kVA, i.e., torque per kVA and power per kVA, shows HA and HC in top due to their low voltage input, i.e., high number of turns. However, looking at the utilization of current density, SynRel topologies have the highest power per current density similar to the non-PM topologies values. Higher torque per current density is also found in the SynRel topologies. This shows how the SynRel differs from the IPM by higher utilization of the reluctance torque.

A summary of the performance of the compared machines:

- NL has the highest power density and moderate current density, however, it lacks in size and power per volume.
- CV2 has a high power density and power per volume, CV2 is the only topology employing ferrite magnets, the low mass density of the ferrite leading to a small total weight. Additionally, the high current density contributes to the higher power capability.
- Small and consequently light-weighted machines are the TP1 and TP2. This leads to high power and torque density as well as high torque per volume. However, small size with high power density makes these machines prone to high temperature rise.
- PM-assisted SynRel topologies have the highest power density and power per volume as well as torque density and torque per volume. The performances come with moderate current density and therefore manageable temperature rise. Additionally, these topologies have good utilization of the current density, i.e., power and torque per current density.
- Magnet-less topologies, i.e., RZ and TS, can achieve good power and torque densities. However, rotor temperature is expected to be an issue for such machines due to the active copper in the rotors. Nevertheless, RZ wound field machine has the advantage of variable field current and therefore better field weakening capability at the expense of commutator complexity and losses.
- Naturally cooled machines, i.e., HC and HA, have low power and torque density. Additionally, SPM topologies suffer from low field weakening capability making them not suitable for a wide speed range application. However, the lack of active cooling reduces the system's complexity and weight.
- BI machine has low current density and therefore possibly does not require a cooling system. However, high power and torque density have been achieved by additional active material in the machine. Similar to the HC and HA, the lack of active cooling reduces the system's complexity and weight.

3 Results summery

A summary of the performance of the compared machines:

- NL has the highest power density and relatively moderate current density and consequently temperature rise, however, it lacks in torque density and torque per volume compared to other PM machines.
- CV2 has a high power density and power per volume, CV2 is the only topology employing ferrite magnets, the low mass density of the ferrite leading to a small total weight. Additionally, the high current density and the required intensive cooling of CV2 contribute to the higher power capability. However, mechanically, high stress due to the rotor geometry limits the speed capability.
- Small and consequently light-weighted machines are the TP1 and TP2. This leads to high power and torque density as well as high power and torque per volume. However, small size with high power density makes these machines prone to high temperature rise. The small rotor diameter reflects well on the mechanical performance making the stress very low and allows for higher speed operation.
- PM topologies with IPM and PMSR rotor configurations have the highest power density and power per volume as well as torque density and torque per volume. The performances come with moderate to high current density and therefore manageable temperature rise with intensive cooling methods. Additionally, these topologies have good utilization of the current density, i.e., power and torque per current density. However, the rotor geometry in some of the PM machines results in high mechanical stress and hence limits the speed range.

Table 1 Electric motors of hybrid and electric vehicles used in the study

Vehicle	Year	Type	Acronym
Honda Accord	2005	Hybrid	HA
Honda Civic	2005	Hybrid	HC
Toyota Prius	2010	Hybrid	TP1
Toyota Prius	2018	Hybrid	TP2
Chevrolet Volt	2016	Hybrid	CV1
Chevrolet Volt	2016	Hybrid	CV2
BMW i3	2014	Full electric	BI
Nissan Leaf	2012	Full electric	NL
Renault Zoe	2014	Hybrid	RZ
Tesla Model S	2012	Full electric	TS

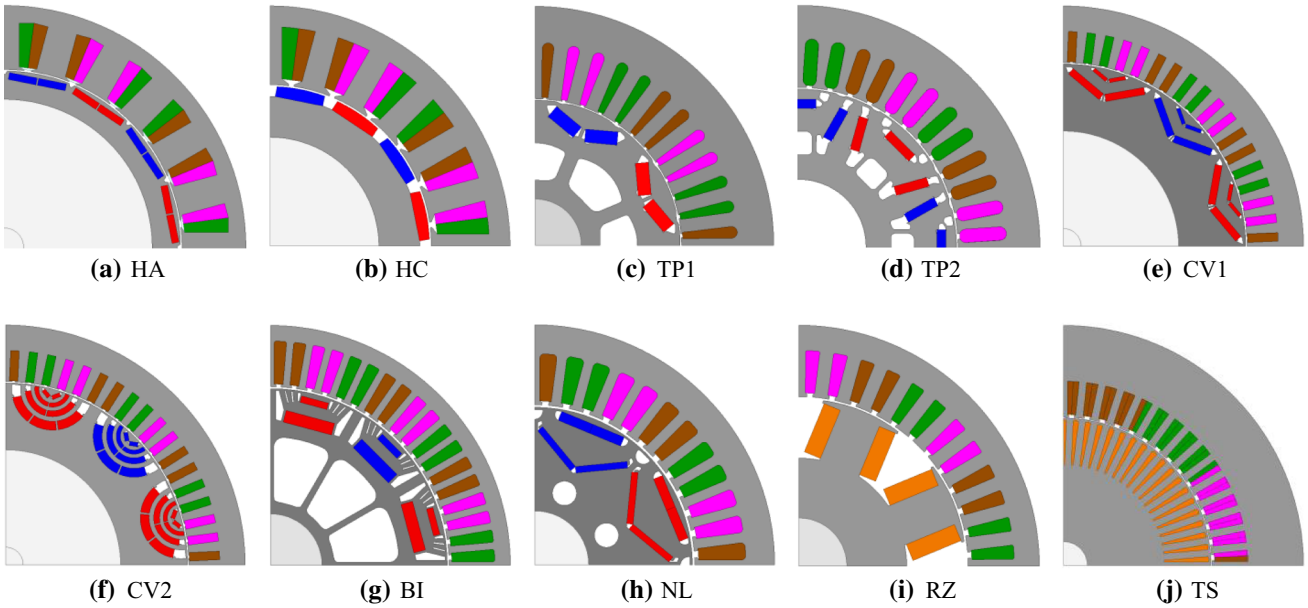

Fig. 1 Cross sections of the studied machines. (**a**) HA (**b**) HC (**c**) TP1 (**d**) TP2 (**e**) CV1 (**f**) CV2 (**g**) BI (**h**) NL (**i**) RZ (**j**) TS

Table 2 Design parameters and specifications of the studied machines

Specifications	HA	HC	TP1	TP2	CV1	CV2	BI	NL	RZ	TS
Topology	SPM	SPM	IPM	IPM	IPM	PMSR	PMSR	IPM	FW	IM
Winding type	C-DL	C-DL	D-SL	D-SL	D-SL	D-SL	D-SL	D-SL	D-SL	D-DL
Coils per phase	8	8	8	8	12	12	12	8	8	12
Turns per coil	52	55	11	4	4	4	6	6	6	1
Parallel paths	8	8	1	1	1	1	3	2	2	2
Peak current density (A/mm^2)	10.9	13.5	43.3	59.9	25.3	25.3	16.8	31.4	26.7	24.24
Peak phase current (A)	225	250	235	700	325	325	400	480	480	900
DC bus voltage (V)	144	144	650	200	360	360	380	360	360	360
Drive kVA	32.4	36	152	140	117	117	141	168	172	324
Stator slots	24	24	48	48	72	72	72	48	48	60
Rotor pole pairs	8	8	8	8	12	12	6	4	8	4
Stator outer diameter (mm)	335	265	264	214	340	340	242	198.12	250	254
Axial length (mm)	40	40	50.8	60	51.5	31.5	132	151.16	155	152
Total active volume (mm^3 E06)	3.53	2.21	2.78	2.16	4.68	2.86	8.56	4.93	7.61	7.7
Permanent magnet weight (kg)	0.79	0.79	1.39	0.66	4.2	0.9	2	1.7	–	–
Armature winding copper weight (kg)	5.5	4.7	0.78	3	1.53	4.1	7.1	4.7	6.09	6.75
Rotor copper weight (kg)	–	–	–	–	–	–	–	–	3.4	6.67
Steel weight (kg)	13.2	8.7	13.9	11.5	21.5	11.9	32.3	24.3	36.4	45.9
Total motor weight (kg)	22.86	18.22	19.08	15.9	30.15	19.6	42	33.1	48.6	60.3

C-DL concentrated double layers, *D-SL* distributed single layer, and *D-DL* distributed double layers

- Magnet-less topologies, i.e., RZ and TS, can achieve good power and torque densities. However, rotor temperature is an issue for such machines due to the active copper in the rotors. Nevertheless, RZ wound field machine has the advantage of variable field current and therefore better field weakening capability at the expected expense of commutator complexity and losses.

Table 3 Performance summary of the studied machines

Performance	Unit	HA	HC	TP1	TP2	CV1	CV2	BI	NL	RZ	TS
Cogging torque (pk-pk)	Nm	10.97	8.97	1.31	0.53	3.34	0.45	2.6	18.8	16.19	–
Back-EMF fundamental, at rated speed	V	111.3	113.6	146.2	41.6	174.6	34.9	116.7	127.09	185.9	–
Back-EMF THD, at rated speed	–	6.03	9.18	17.45	8.8	14.74	15.11	11.2	9.19	15.94	–
Torque ripple, at peak current	–	18.47	3.51	9.79	31.2	21.65	28.78	25	10.9	27.03	8.99
Average torque, at peak current	Nm	119.5	122.8	227.9	191	309.8	130.1	300	314.7	339	330
Torque per volume	Nm/mm^3E06	33.88	55.57	81.98	88.4	66.20	45.51	35	63.85	44.56	42.8
Torque density	Nm/kg	5.22	6.73	11.9	12	10.27	6.63	6.45	9.5	6.97	5.47
Torque per KVA	Nm/kVAE03	3.69	3.41	1.5	1.36	2.65	1.11	2.12	1.87	1.97	1.01
Torque per magnet weight	Nm/kg	151.2	155.4	163.9	289	73.76	118.2	93.75	185	–	–
Torque per current density	$Nm/A/mm^2$	10.97	9.10	5.26	3.18	12.25	5.15	17.8	10.03	12.70	13.61
Maximum output power	kW	27.2	31	77	68.4	100.4	78.2	121	154	90.2	250
Power per volume	kW/mm^3E06	7.71	14.03	27.69	31.6	21.45	27.34	14	31.24	11.85	32.4
Power density	kW/kg	1.18	1.7	4.03	4.3	3.3	3.9	2.6	4.65	1.85	4.1
Power per KVA	kW/kVA	0.84	0.86	0.5	0.48	0.86	0.67	0.85	0.92	0.52	0.77
Power per magnet weight	kW/kg	34.4	39.2	55.39	103.6	23.9	86.8	37.8	90.5	–	–
Power per current density	$kW/A/mm^2$	2.50	2.30	1.77	1.14	3.97	3.09	7.14	4.90	3.38	10.31

- Naturally cooled machine, i.e., HC, and less complex cooled, i.e., HA, have low power and torque density. Additionally, SPM topologies suffer from low field weakening capability making them not suitable for a wide speed range application.
- BI machine has low current density and therefore less complex cooled. However, the high power and torque have been achieved by additional active material in the machine.

Furthermore, to summarize the outcome of the comparative study, Fig. 2 presents the trend of the torque density, power density, the rotor peripheral speed, rotor mechanical stress, and the required cooling methods under conventional and hairpin winding arrangements. The peripheral speed is calculated at the machine's base speed and the mechanical stress is predicted at speed of 15krpm.

From Fig. 2, it can be seen that the current limit of the torque and power densities are 13Nm/kg and 4.5 kW/kg, respectively. Moreover, along the timeline, the increase in the torque and power density are in-line with the increase in the more aggressive cooling methods. Similarly, the increase in the rotor mechanical stress and peripheral speed along the timeline is in-line with the torque and power densities.

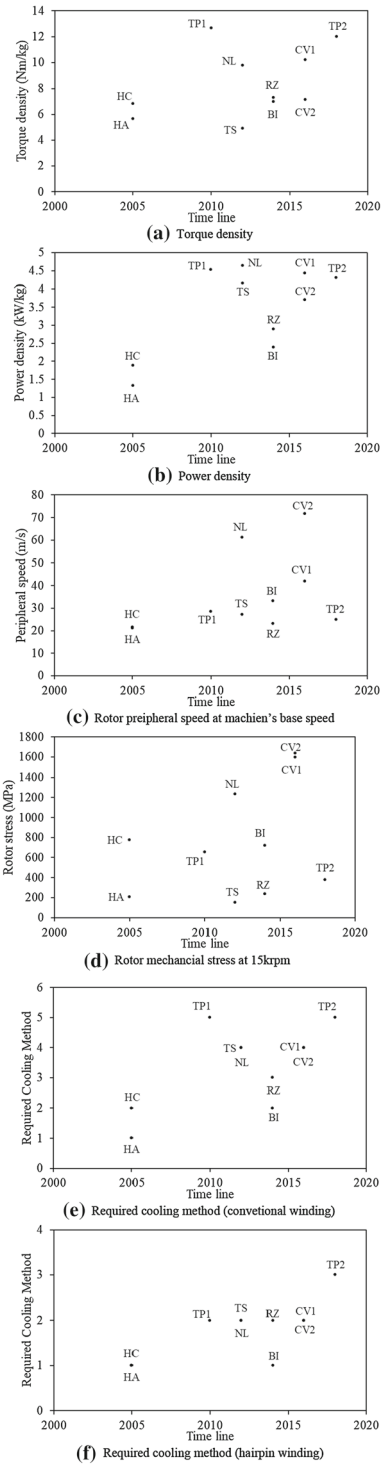

Fig. 2 The trend of electrical machines in EVs and HEVs. (**a**) Torque density (**b**) Power density (**c**) Rotor peripheral speed at machine's base speed (**d**) Rotor mechanical stress at 15 krpm (**e**) Required cooling method (conventional winding) (**f**) Required cooling method (hairpin winding)

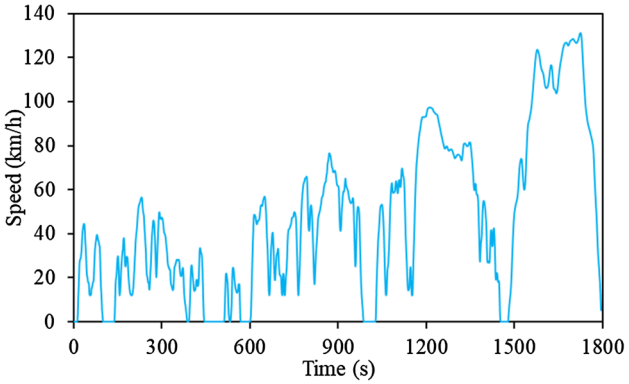

Fig. 3 WLTP driving cycle

Table 4 Electrical machine targets by the APC and FC [17, 18]

Performance	FC 2020	APC 2025	APC 2035
Continuous power density (kW/kg)	0.86	7	9
Continuous power per volume (kW/mm^3 E06)	1.82	25	30
300% material cost ($/kW)	33.25	5.8	4.5
WLTP drive cycle efficiency	82	92.5	93
DC voltage (V)	NS	350	350
Current (A)	NS	450	450
Cooling inlet temperature (C)	70	65	65

*NS not specified

4 New design criteria for future automotive

By the end of 2019, light-duty vehicles registered in the EU, Switzerland, Norway, Iceland and Turkey must comply with the worldwide harmonized light vehicle test procedure (WLTP) driving cycle as a replacement for the new European driving cycle (NEDC). Figure 3 presents the class 3 WLTP drive cycle [16].

The UK advance propulsion center (APC) has summarized the requirements for electric motors in automotive to meet the legislative requirements of 2025 and 2035 as shown in Table 4 [17]. Similarly, the USA equivalent, FreedomCar (FC), published the criteria for 2020 [18]. Considering a maximum output power of 100 kW, the required torque-speed characteristic to meet the requirements have been predicted for different gearbox ratios and presented in Fig. 4. This summarizes the targets for electrical machine design for automotive to meet the 2035 performance requirement. Cost requirements and material suitability, on the other hand, are

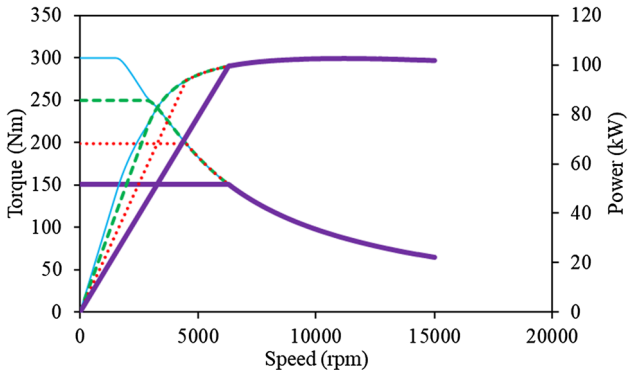

Fig. 4 Predicted torque-speed characteristics for future electrical machines in automotive

more difficult to quantify, however, rare-earth-free, low-cost steel grade and low copper consumption are targets to be considered in the design of electric machines for automotive.

5 Designing techniques

This section explores and presents different electrical machine design techniques that can help electrical machine designers to reach the future requirements for electric motors in automotive.

5.1 Cooling system

To explore the different electrical machine cooling systems and their heat removal capability, a study has been made using the ten compared machines. The study consists of employing different cooling systems on the machines and observe the temperature in the winding, steel and PM of the machine.

The temperature rise has been predicted using a combined LPC model and mathematical thermal calculations. Different cooling methods have been evaluated on all the machines as shown in Table 5. This is to have a fair comparison of the thermal capability of the different topologies as cooling specifications of some of the machines are not available in the literature. Neutral cooling, stator jacket, stator jacket with spray cooling and stator slot channels have been investigated. Figure 5 presents and illustrates the four methods. The calculation is made at peak conditions with a transient of 1200 s and 3000 rpm, and a flow rate of 6 l/min of EGW50/50 cooling oil.

Both HA and HC operate with low current density, therefore, natural air cooling is suitable to maintain the machine temperature around 200 °C. Therefore, with a high temperature magnet grade and winding with insulation class 4 the machine can operate with natural convection. Similarly, the low current density of BI makes it operational with only natural convection.

TP1 and TP2 have the highest current density and consequently copper loss making the temperature rise extremely high. A stator slot channels cooling is therefore required to bring down the winding temperature. Similarly, CV1, CV2 and NL have high current density leading to the need for excessive cooling of both spray and stator jacket or stator slot channels cooling.

Table 5 Temperatures (°C) in different motor parts under different cooling methods

		Natural convention	Stator jacket	Stator jacket-spry cooling	Stator slot cooling
HA	Winding	183	120	106	82
	Magnet	181	120	58	120
	Steel	175	113	78	118
HC	Winding	226	160	146	82
	Magnet	172	122	43	106
	Steel	202	123	102	100
TP1	Winding	997	664	659	318
	Magnet	406	225	46	124
	Steel	749	464	396	136
TP2	Winding	1580	1196	865	480
	Magnet	620	348	80	191
	Steel	1099	603	402	240
CV1	Winding	471	305	243	178
	Magnet	241	135	43	114
	Steel	378	199	146	127
CV2	Winding	480	316	242	180
	Magnet	260	139	42	117
	Steel	390	216	150	122
BI	Winding	242	117	75	78
	Magnet	128	78	45	60
	Steel	226	102	65	63
NL	Winding	489	254	246	152
	Magnet	183	106	45	70
	Steel	411	174	148	80
RZ	Winding	378	213	198	136
	Rotor winding	292	212	77	174
	Steel	324	158	126	161
TS	Winding	373	276	240	180
	Rotor cage	252	215	112	189
	Steel	285	183	148	185

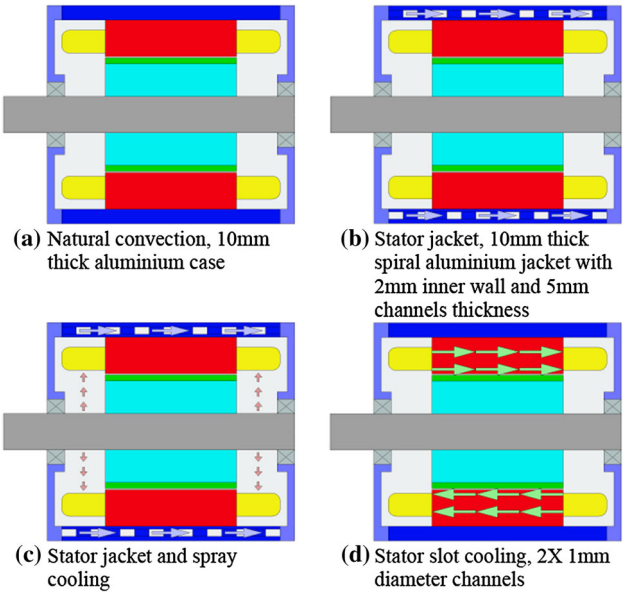

Fig.5 Illustration of the cooling methods. (**a**) Natural convection, 10 mm thick aluminum case (**b**) Stator jacket, 10 mm thick spiral aluminum jacket with 2 mm inner wall and 5 mm channels thickness (**c**) Stator jacket and spray cooling (**d**) Stator slot cooling, 2X 1 mm diameter channels

Magnet-less topologies in RZ and TS have high current density and therefore stator jacket or stator slot channels cooling is required. However, the active field winding and induction cage in the rotor leading to the need for rotor cooling. Therefore, spray cooling is a suitable solution. However, TS uses active shaft cooling [14].

5.2 Hairpin winding

The technology of hairpin winding allows for an automated winding process of the machine and the large rectangular coils achieve a high winding filling factor and therefore allow for more current or lower loss density. However, low number of turns and high AC loss are drawbacks of hairpin winding that are not very effective in automotive since relatively low number of turns are used and the moderate speed renders AC loss as insignificant.

The hairpin winding has been studied through employing such windings in the studied machines and compare them with their original counterparts. Original stator and parallel slot of each machine have been studied. Figure 6 presents an illustration of the conventional and hairpin winding. The fill factor and winding temperature rise are presented and compared in Table 6. Hairpin winding can be made with a low number of turns, current products are made with up to 6 turns [19], therefore, TP2 turns has changed from 11 to 4 turns and consequently the current changed from 235A to 646.25A to maintain the same current density and ampere-turn. Similarly, HA turns changed to 2 turns and the current

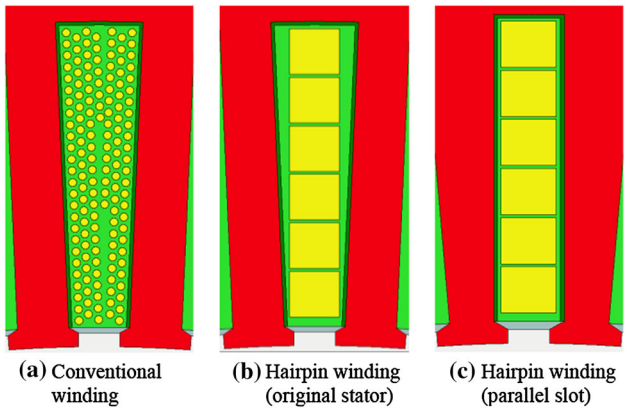

Fig. 6 Conventional and hairpin winding illustration. (**a**) Conventional winding (**b**) Hairpin winding (original stator) (**c**) Hairpin winding (parallel slot)

to 5850A, HC turns changed to 2 turns and the current to 6875A.

5.3 Mechanical rotor design

To achieve high performance, in particular power density, high speed and a large rotor diameter are both used. This places a high demand on innovative rotor geometry to keep the mechanical stresses with the acceptable limits of the used material. To examine the mechanical capability of different rotor topologies, the radii of the investigated machine's rotors have been changed to 100 mm. Table 7 lists the maximum stress and deformation of each of the rotors.

From the comparison, the highest stresses are exhibited by NL, this is due to the location of a thick magnet near the rotor surface. The rotor core that holds this magnet is under high stress due to the high deformation at the center as shown in Fig. 7. This can be avoided by multi-layer magnets having the smallest near the surface like in CV1, CV2 and BI. In addition, these machines have inner ribs between or at the sides of the larger magnets to reduce the deformation along the center. However, magnetically these ribs are undesirable due to leakage. Therefore, adding gaps between the magnets and ribs introduces a compromise between mechanical integrity and electromagnetic performance. Finally, the lowest stresses are found in the TP2. This is since the magnet near the surface is placed further inside the core with bridges to withstand deformation. The design provides a balance between mechanical and electromagnetic performance. The side magnets are held with notches instead of full bridges, whereas the core is held by bridges away from the magnets to provide a balance. HA machine encloses the magnets in core pockets with a middle bridge making the mechanical design suitable for maintaining stress low. The sleeve in the HC machine maintain a low stress level in the rotor and the sleeve, however, the process of applying retaining sleeve is considered complex and costly.

Table 6 Comparison of conventional and hairpin winding in different machines, DC loss (W), Temperature (°C)

	Conventional winding			Hairpin winding (original stator)			Hairpin winding (parallel slot stator)		
	*K*p	DC loss	Temp	*K*p	DC loss	Temp	*K*p	DC loss	Temp
HA	0.6	704	106	0.58	733	108	0.77	501	75
HC	0.6	888	146	0.5	927	148	0.75	707	102
TP1	0.4	7952	659	0.5	6033	384	0.75	3123	162
TP2	0.4	11,130	865	0.53	7883	528	0.72	5345	278
CV1	0.4	3981	243	0.56	2802	168	0.7	2035	124
CV2	0.4	3098	242	0.56	2455	180	0.7	1760	124
BI	0.4	2405	75	0.5	1914	68	0.63	1648	62
NL	0.4	5059	246	0.48	4165	216	0.62	3670	166
RZ	0.4	4292	198	0.48	3530	181	0.63	2787	131
TS	0.4	4390	240	0.55	3124	128	0.69	2782	112

Table 7 Maximum stress and deformation of the investigated machines with 100 mm radius and at 15 krpm

	HA	HC	CV1	CV2	TP1
Stress (MPa)	398.5	184.6	960.3	1008	1007
Deformation (mm)	0.015	0.091	0.031	0.054	0.064
	TP2	BI	NL	RZ	TS
Stress (MPa)	811.1	876.7	2917	314.1	246.2
Deformation (mm)	0.065	0.093	0.33	0.02	0.03

Finally, both the RZ and TS rotors have low stresses. This is since the large RZ rotor teeth hold the winding. Similarly, the TS rotor core has a large core frame surrounding the copper cage.

On the other hand, the magnets are brittle with low yield/tensile strength, therefore, they need to be carefully retained. Enclosing the magnets by the rotor core and end-caps ensures mechanical safety since no space is allowed for magnet deformation. Additionally, in the case of breakage, the magnet fragments will remain in their location and this will not inhibit the machine's performance. Gaps between the magnet and core can be filled with epoxy to maintain a full magnet enclosure. Other techniques to reduce magnet stress is corner gaps as highlighted in Fig. 8. Such gaps allow magnet deformation at the point of maximum impact with the rotor core under rotational forces.

5.4 Reduced rare-earth, rare-earth-free and magnet-less topologies

From the comparison summary, it has been seen that magnet-less topologies with an active rotor suffer from high weight and therefore low power density and the need for rotor cooling. On the other hand, magnet-less topologies with a passive rotor, i.e., synchronous and switched reluctance have inertly low power density. Figure 9 presents the cross section and torque-speed curve for a switched reluctance (SR) machine designed for an automotive application, while Table 8 lists key specifications. It can be seen that the power density is low. Additionally, the need for a high number of slot leads to concentrating the copper loss across a larger area making it difficult to extract the heat.

Reduced-rare-earth (RRE) and rare-earth-free (REF) are a positional solution to the cost and power density requirements. RRE is the topologies with a combination of NdFeB and ferrite [20]. This allows for a relatively high magnetic loading and avoids demagnetization of ferrite magnets while reducing the consumption of the rare-earth material. However, the need to replace rare-earth with sustainable materials makes this approach a short term solution.

REF CV2 machine has an identical stator to the CV1 with shorter axial length and less power. To investigate the capability of REF machine, the CV2 axial length has been changed to compare the performance of both machines at the same size and same output torque, i.e., increased axial length to match the torque of the CV1 machine. Figure 10 presents the torque-speed and power speed curves of the CV1 (51.5 mm axial

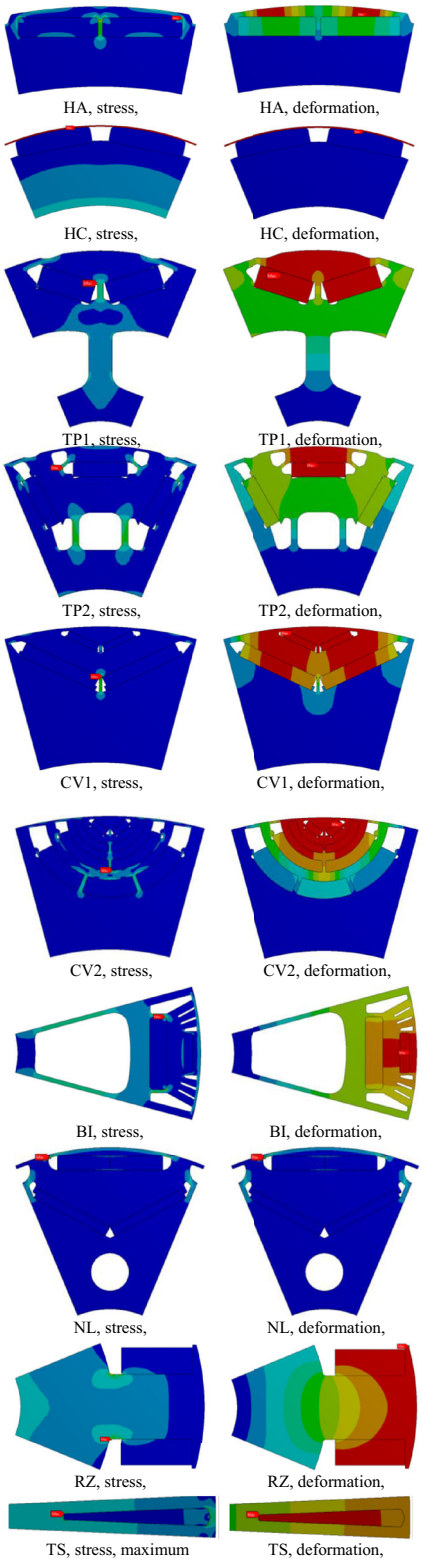

Fig. 7 Mechanical stress and deformation distribution in the studied machines

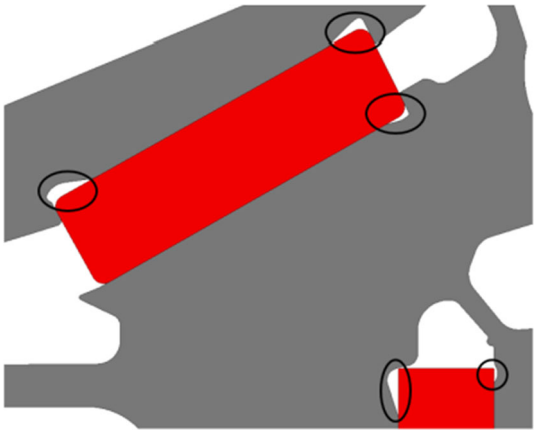

Fig. 8 Magnet-core gaps to reduce the stress on the magnet

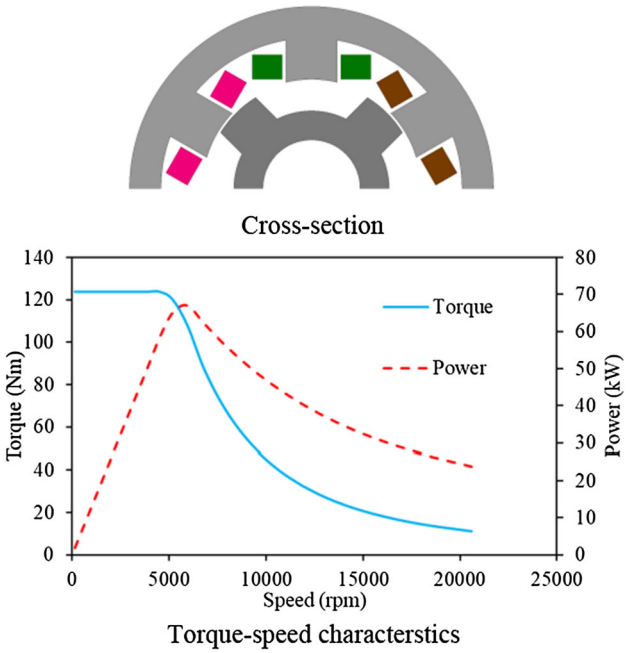

Fig. 9 SR Machine cross section and torque-speed curve

Table 8 Key specifications of SR machine

Specifications and performance	Value
Outer diameter (mm)	150
Airgap (mm)	1
Axial length (mm)	260
Power density (kW/kg)	1.05
Maximum temperature (°C)	198

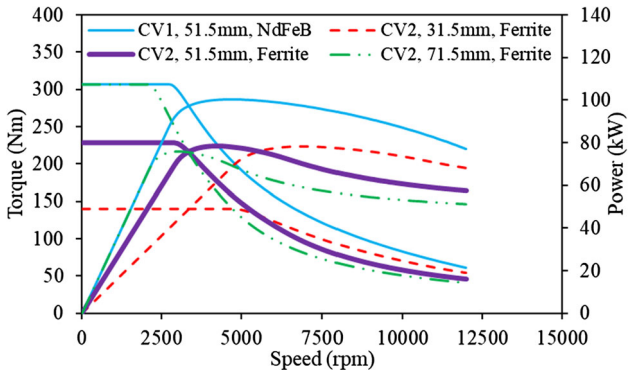

Fig. 10 Torque-speed characteristics of CV1 and CV2 machines with different axial lengths

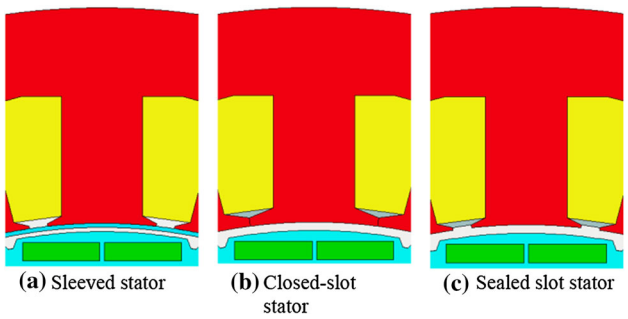

Fig. 11 Illustration of stator slot opening for semi-flooded cooling. (**a**) Sleeved stator (**b**) Closed-slot stator (**c**) Sealed slot stator

length), CV2 (31.5 mm axial length), CV2 with 51.5 mm axial length and CV2 with 71.5 mm axial length.

5.5 Aggressive cooling

The key to high power density is a smaller machine with a higher current density. A small, lightweight machine needs a high current density to match the automotive target, therefore, high loss density and consequently heat is expected. Mechanically, the small size allow for higher speeds due to the small rotor diameter.

The answer for excessive cooling is fully flooded and semi-flooded methods. The first being undesirable due to the high wind age loss. Semi-flooded cooling has been used in the aerospace applications and the research has matured this technology to a practical level [21]. The challenges with semi-flooded cooling are mechanical and assembly rather than theoretical design issues. Elimination of fluid leakage and sealing of the system are the main challenges.

To examine the effectiveness of the semi-flooded cooling, a study on the compared machines have been conducted. The theoretical design of a semi-flooded cooling has been illustrated in [22]. A separation sleeve between the stator and rotor, i.e., placed in the airgap is required. The thickness of the sleeve is determined based on the flow rate of the fluid and the slot opening thickness. Similar to retaining sleeves in high speed machines, the sleeve needs to be made of a non-magnetic, non-electrically conductive material to avoid electromagnetic and losses issues. A closed-slot machine could be a solution to avoid the sleeve and consequently increasing the airgap length. Closed-slot technique has been proposed and employed in high-speed machines to reduce the space harmonics [22]. However, closed-slot stator suffers from high voltage spikes as stated in [23], which affect the torque-speed characteristics. Coincidentally, a higher number of stator slots diminishes this effect as stated in [23]. Additionally, flux leakage through the closed-slot tip leads to lower torque and influences the torque-speed characteristics. This can be avoided by using heat treatment electrical steel, i.e., dual phase steel [24], however, the low magnetic properties of such steel can be a challenge.

Theoretically, the most electromagnetically suitable design for a semi-flooded machine is a conventional stator with open slots and no sleeve in the airgap, i.e., small electromagnetic airgap and no stator flux leakage. This can be achieved assuming sealing techniques are applied to close the stator opening and prevents any fluid leakage. Semi-flooded cooling has been studied on the compared machines using sleeve, closed-slot and sealed slot stator. A sleeve of 1 mm made of carbon fiber is used in the machines, therefore the airgap increased by 1 mm at the expense of the rotor. Similarly, a closed-slot of 1 mm tooth-tip has been used. Figure 11 presents the illustration of the sleeved stator, closed-slot and sealed slot. Table 9 presents the results.

5.6 Design to recycle

Although this aspect has not been introduced as a mandatory requirement for EV and HEV, the latest legislative requires more than + 80% of the vehicle to be recyclable. This has been specified in from of recyclable materials. The recycling of electric machines and consequently design-to-recycle (DtR) has been briefly explored in the literature of electrical machine design [25]. The recycling aspect of an electrical machine is divided into recyclable materials and recyclable designs. The first refers to using materials that are recyclable and the second refers to using design techniques to avoid high integration of the different parts and materials of the electrical machine and easy disassembly.

Recyclable materials: Aluminum versus copper winding; aluminum being the most widely recyclable material making aluminum windings a main DtR technique. Aluminum windings have been proposed and studied for high-speed machines due to the better AC/DC loss ratio. However, for moderate speed machines like in automotive applications aluminum winding means higher winding loss and temperature rise.

Table 9 Comparison of torque (Nm) and temperature (°C) in semi-flooded machines with sleeved stator, closed-slot stator and sealed slot stator

	Sleeved stator		Closed-slot stator		Sealed slot stator	
	Torque	Temp	Torque	Temp	Torque	Temp
HA	98.5	58	115	61	119.5	60
HC	106.8	68	115	70	122.8	68.9
TP1	152.64	136	166.8	136	176.8	136
TP2	164.6	193	177.2	192	188	192
CV1	256.98	77.5	302.4	79	309.8	78.9
CV2	100	78	125	79	130.1	79
BI	190	55	220	57.5	236.8	57
NL	271.7	97	310	98	314.7	98
RZ	272.78	87	335	83	339	89
TS	385	80	395	80	400	80

Aluminum hairpin winding can help introducing aluminum into automotive electrical machines since the higher filling factor can compensate for the higher winding loss. Similar to ferrite, the low cost and low mass density of aluminum are additional merits.

Silicon-contained laminated steel versus solid steel; according to [25], silicon-contained laminated steel became unrecyclable due to the contamination with adhesive. Therefore, soft magnetic composite (SMC) and solid steel are suitable solutions for electrical machine core recyclability. However, in addition to the low magnetic properties, the SMC is a brittle material with low mechanical strength. This makes the SMC unsuitable automotive. On the other hand, solid steel has main challenges of low magnetic properties and high eddy current losses which require several techniques to overcome [26]. The non-coated Ferrite/SmCo versus the coated NdFeB; due to the need for coating, NdFeB magnets are very difficult to recycle due to the high coating contamination [25]. A recycled NdFeB has half the magnetic performance of newly made magnets [2]. Therefore, non-coated SmCo and ferrite are easier to recycle. As shown in Section C, Ferrite has shown good potential for automotive. The recyclability is additional merit to the low cost and weight. On the other hand, SmCo has very similar magnetic capability to the NdFeB and higher capability to withstand higher temperature. However, the high cost of SmCo magnet compared to NdFeB is the main disadvantage.

Recyclable designs: Coating, adhesive and varnish; to recycle a material, the purity of the material is the main object. Therefore, the use of coating, adhesive and varnish would contaminate the materials and removing them and separating them from the other materials is a very difficult process that might not be even possible. Therefore, a DtR machine must contain a reduced or eliminated coating, adhesive and varnish.

Disassembly: an easy to disassemble design is required for recycling. The ability to assemble the different parts without high integration and therefore separate the different components easily.

To explore the DtR aspects, aluminum winding and solid steel have been employed in the studied machines. Table 10 compares the original machines with the same machine albeit of aluminum winding in conventional and hairpin (parallel slot) configurations. The higher power density due to the low mass density of aluminum is the main advantage, the increase in winding loss and consequently the temperature can be avoided by using hairpin winding. Aluminum hairpin winding show the advantages of low AC loss which brings the total winding loss close to its counterpart copper hairpin. On the other hand, solid steel suffers from low B-H curve which results in lower torque. It is worth noting the solid steel suffers from large eddy currents which consequently lead to high loss and disturbance in the magnetic performance, especially if used in the stator. However, the large eddy current can be mitigated using axial segmentation or slitting [26].

5.7 Multi-objective optimization

Although this aspect has not been introduced as a mandatory requirement for EVs, the optimization of electric vehicle seeks to reduce the amount of energy used while simultaneously enhancing their driving capabilities and keeping their costs and weight to a minimum. Because there is no one optimal solution that can satisfy all of these competing objectives, it is essential that the issue be formulated to take into account all of them at the same time. The term "multi-objective optimization," refers to a technology that helps find the optimum solutions that compromise many goals [27, 28].

The multi-objective optimization is another research hotspot. The most common and widely used method for optimizing electrical machines is performed using finite element

Table 10 Comparison of copper and aluminum winding, (AC loss at 5000 rpm), Cu/Al: conventional copper/aluminum winding and CuH/Alh: hairpin copper/aluminum winding. DC loss (W), AC loss (W), Temperature (C), weight (kg)

		*K*p	DC loss	AC loss	Total loss	Max Temp	Total weight	Max winding
HA	Cu	0.6	704.3	446	1150.3	150	106	22.86
	Cuh	0.77	501	3059	3560	217	75	24.98
	Al	0.6	1148	274	1422	168	135	19.07
	Alh	0.77	802	2369	3171	202	87	19.53
HC	Cu	0.6	888	478	1366	214	146	18.22
	Cuh	0.75	707	4029	4736	365	102	19.48
	Al	0.6	1448	293	1741	248	199	14.93
	Alh	0.75	1152	3157	4309	340	132	15.32
TP1	Cu	0.4	7952	246	8198	679	659	19.08
	Cuh	0.75	3123	2943	6066	313	162	23.53
	Al	0.4	12,960	151	13,111	1104	1107	16.51
	Alh	0.75	5347	2306	7653	379	286	17.26
TP2	Cu	0.4	11,130	930	12,060	905	865	15.33
	Cuh	0.72	5345	3560	8905	420	278	18.64
	Al	0.4	18,130	578	18,708	1455	1280	13.25
	Alh	0.72	8900	2331	11,231	525	421	13.82
CV1	Cu	0.4	3981	920	4901	350	243	30.15
	Cuh	0.7	2035	2640	4675	217	124	33.89
	Al	0.4	6487	673	7160	478	370	27.22
	Alh	0.7	3315	2068	5383	240	168	28.14
CV2	Cu	0.4	3442	541	3983	353	242	19.61
	Cuh	0.7	1760	1383	3143	187	124	22.53
	Al	0.4	5608	395	6003	495	367	16.79
	Alh	0.7	2866	1084	3950	220	177	17.55
BI	Cu	0.4	2405	2446	4851	90	75	46.51
	Cuh	0.63	1648	1859	3507	75	62	50.79
	Al	0.4	3918	1589	5507	117	103	41.12
	Alh	0.63	2692	1208	3900	92	76	43
NL	Cu	0.4	5059	696	5755	286	246	33.17
	Cuh	0.62	3670	983	4653	199	166	35.71
	Al	0.4	8244	427	8671	441	411	29.9
	Alh	0.62	5732	603	6335	269	246	31
RZ	Cu	0.4	4292	1083	5375	242	198	48.68
	Cuh	0.63	2787	1699	4486	195	131	51.93
	Al	0.4	7005	663	7668	354	330	44.49
	Alh	0.63	5029	1041	6070	241	270	46.09
TS	Cu	0.4	4390	344	4734	246	240	60.32
	Cuh	0.69	2782	1657	4439	133	112	65.09
	Al	0.4	7153	211	7364	465	441	55.68
	Alh	0.69	4328	1298	5626	174	157	57.4

analysis (FEA) coupled with optimization algorithms such as genetic algorithm (GA) [29–31], particle swarm optimization (PSO) algorithm [32–34], nondominated sorting genetic algorithm-II (NSGA-II) [35, 36], fuzzy method, and sequential Taguchi method [37, 38]. In addition, the application of multilevel optimization strategy is a promising method for efficient multi-objective optimization, in particular for the optimization methods that need to effectively solve the multi-parameter and multi-objective optimization problems [39].

The aforementioned methodologies have the potential to be used for the purpose of effective multi-objective optimization of electrical machines with high dimensions for applications in the automotive industry.

6 Conclusion

This paper presents a comparison of the state-of-art electrical machines and design techniques used in automotive. Ten designs based on the market available literature have been compared, these machines have different topologies and specifications. From this comparison machines with PM-assisted SynRel topologies have the highest power density and power per volume as well as torque density and torque per volume.

The future targets for electrical motors in automotive applications are illustrated by highlighting the advanced propulsion center (APC) targets for 2035, predicting a torque-speed profile and working toward the WLTP driving cycle. Furthermore, state-of-art design techniques have been studied through employing them in the various topologies to highlight the influence of such techniques and their ability to bring the designs to future targets. The investigated techniques are hairpin winding, rotor mechanicals, complex cooling, recyclable design, and reduced and rare-earth free machines. Hairpin winding provides a significant reduction in loss density of the winding and higher thermal dissipation. Therefore, a lower temperature rise and hence smaller size and higher power density can be achieved with hairpin winding. Complex cooling such semi-flooded allows for high heat removal from the stator winding allowing higher current density and consequently higher power density. However, issues of airgap sleeve and sealing reduce the performance of the machine and add assembly complexity. Rare-earth free machines, i.e., ferrite, have a potential for automotive. The low mass density allows for less weight, however, the weak coercivity of the ferrite make it easier to field weakening and hence a field weakening higher than 1 is normally found, this reduces the wide power capability over the speed range. Finally, aluminum hairpin winding is a promising for design recyclability in addition to the lower AC loss, lower weight and cost benefits.

Open Access This article is licensed under a Creative Commons Attribution 4.0 International License, which permits use, sharing, adaptation, distribution and reproduction in any medium or format, as long as you give appropriate credit to the original author(s) and the source, provide a link to the Creative Commons licence, and indicate if changes were made. The images or other third party material in this article are included in the article's Creative Commons licence, unless indicated otherwise in a credit line to the material. If material is not included in the article's Creative Commons licence and your intended use is not permitted by statutory regulation or exceeds the permitted use, you will need to obtain permission directly from the copyright holder. To view a copy of this licence, visit http://creativecommons.org/licenses/by/4.0/.

References

1. Zeraoulia M, Benbouzid MEH, Diallo D (2006) Electric motor drive selection issues for HEV propulsion systems: a comparative study. IEEE Trans Veh Technol 55(6):1756–1764
2. Kimiabeigi M et al (2018) Production and application of HPMS recycled bonded permanent magnets for a traction motor application. IEEE Trans Ind Electron 65(5):3795–3804
3. Olszewski M (2006) Evaluation of the 2005 Honda Accord hybrid electric drive system. Oak ridge national laboratory, ORNL/TM-2006/535. https://www.osti.gov/servlets/purl/891260
4. Olszewski M (2011) Evaluation of the 2010 Toyota Prius hybrid synergy drive system. Oak ridge national laboratory, ORNL/TM-2010/253. https://info.ornl.gov/sites/publications/files/pub26762.pdf
5. Zhu ZQ, Chu WQ, Guan Y (2017) Quantitative comparison of electromagnetic performance of electrical machines for HEVs/EVs. CES Trans Electr Mach Syst 1(1):37–47
6. . Guan Y, Zhu ZQ, Afinowi IAA, Mipo JC Farah P (2014) Design of synchronous reluctance and permanent magnet synchronous reluctance machines for electric vehicle application. *2014 17th International Conference on Electrical Machines and Systems (ICEMS)*, Hangzhou, 2014, pp. 1853–1859.
7. Momen F, Rahman K, Son Y (2019) Electrical propulsion system design of chevrolet bolt battery electric vehicle. IEEE Trans Ind Appl 55(1):376–384
8. Jurkovic S, Rahman K, Bae B, Patel N and Savagian P, (2015) "Next generation chevy volt electric machines; design, optimization and control for performance and rare-earth mitigation," *2015 IEEE Energy Conversion Congress and Exposition (ECCE)*, Montreal, QC, 2015, pp. 5219-5226
9. Anwar, Mohammad, et al. (2015) Power Dense and Robust Traction Power Inverter for the Second-Generation Chevrolet Volt Extended-Range EV. *SAE Int J Altern Powertrains JSTOR*
10. Merwerth J (2014) The hybrid-synchronous machine of the new 642 BMW i3 and i8. BMW group. https://www.speakev.com/20140404_bmw-pdf
11. BMW (2017) Specifications. The new BMW i3. BMW Media Information. https://www.press.bmwgroup.com
12. Staton D and Goss J, (2017) Open Source Electric Motor Models for Commercial EV & Hybrid Traction Motors," 2017 CWIEME, Berlin, 2017.
13. Roggia S and. Iacchetti M, (2016) Open source electric motor models for commercial EV & hybrid traction motors. International conference on electrical machines ICEM, Lausanne,
14. Fedoseyev L, Pearce E (2016) Rotor assembly with heat pipe cooling system. U.S. Patent 2014036806A1
15. Kane M (2015) Renault electric motor production at Cleon. Renault Group. https://www.renaultgroup.com/en/news-on-air/

news/the-cleon-plant-embarks-on-its-industrial-renaulution-and-goes-electric/
16. WLTP Facts, What is WLTP. https://www.wltpfacts.eu/what-is-wltp-how-will-it-work/
17. APC (2020) Electric Machines Roadmap. APC. https://www.apcuk.co.uk/app/uploads/2021/09/https___www.apcuk_.co_.uk_app_uploads_2021_02_Exec-summary-Technology-Roadmap-Electric-Machines-final.pdf
18. US Department of Energy (2011) Hybrid and Electric Propulsion. https://www1.eere.energy.gov/vehiclesandfuels/pdfs/mypp/3-2_hybr_elec_prop.pdf
19. Staton D (2018) Electric motor design: trade-off analysis. CWIEME, Berlin
20. Afinowi IAA, Zhu ZQ, Guan Y, Mipo JC and Farah P (2014) Performance analysis of switched-flux machines with hybrid NdFeB and ferrite magnets. *2014 17th International Conference on Electrical Machines and Systems (ICEMS)*, Hangzhou, pp. 3110–3116.
21. Xu Z et al (2017) A semi-flooded cooling for a high speed machine: concept, design and practice of an oil sleeve. IECON Beijing 2017:8557–8562
22. Papini L, Raminosoa T, Gerada D, Gerada C (2014) A high-speed permanent-magnet machine for fault-tolerant drivetrains. IEEE Trans Ind Electron 61(6):3071–3080
23. Wu D, Zhu ZQ (2015) Influence of slot and pole number combinations on voltage distortion in surface-mounted permanent magnet machines with local magnetic saturation. IEEE Trans Energy Convers 30(4):1460–1471
24. Reddy PB et al (2018) Performance testing and analysis of synchronous reluctance motor utilizing dual-phase magnetic material. IEEE Trans Ind Appl 54(3):2193–2201
25. Alatalo M, Lundmark ST, Emma Arfa Grunditz (2011) Electric machine design for traction applications considering recycling aspects-review and new solution. *IECON 2011*, Melbourne, VIC, pp. 1836-1841
26. Arumugam P et al (2016) High-speed solid rotor permanent magnet machines: concept and design. IEEE Trans Transp Electr 2(3):391–400
27. Al-Ani M et al (2021) Influence of manufacturing and drive effects in high-speed, high-power-density PM machine for flooded pump application. IEEE Workshop Electr Mach Des Control Diagn (WEMDCD). https://doi.org/10.1109/WEMDCD51469.2021.9425659
28. Ramakrishnan K, Stipetic S, Gobbi M and Mastinu G (2016) Multi-objective optimization of electric vehicle powertrain using scalable saturated motor model," Eleventh International Conference on Ecological Vehicles and Renewable Energies (EVER), 2016, pp. 1-6
29. Jannot X, Vannier J, Marchand C, Gabsi M, Saint-Michel J, Sadarnac D (2011) Multiphysic modeling of a high-speed interior permanent-magnet synchronous machine for a multiobjective optimal design. IEEE Trans Energy Convers 26(2):457–467
30. Nakata T, Sanada M, Morimoto S, Inoue Y (2017) Automatic design of IPMSMs using a genetic algorithm combined with the Coarse-mesh FEM for enlarging the high-efficiency operation area. IEEE Trans Ind Electron 64(12):9721–9728
31. Rostami N, Feyzi MR, Pyrhonen J, Parviainen A, Behjat V (2012) Genetic algorithm approach for improved design of a variable speed axial-flux permanent-magnet synchronous generator. IEEE Trans Magn 48(12):4860–4865
32. Dong F, Zhao J, Song J, Feng Y, He Z (2018) Optimal design of permanent magnet linear synchronous motors at multispeed based on particle swarm optimization combined with SN ratio method. IEEE Trans Energy Convers 33(4):1943–1954
33. Lee JH, Song J, Kim D, Kim J, Kim Y, Jung S (2018) Particle swarm optimization algorithm with intelligent particle number control for optimal design of electric machines. IEEE Trans Ind Electron 65(2):1791–1798
34. Lin F, Teng L, Chu H (2008) A robust recurrent wavelet neural network controller with improved particle swarm optimization for linear synchronous motor drive. IEEE Trans Power Electron 23(6):3067–3078
35. Bu J, Lan X, Zhou M, Lv K (2018) Performance optimization of flywheel motor by using NSGA-2 and AKMMP. IEEE Trans Magn 54(6):1–7
36. Bu J, Zhou M, Lan X, Lv K (2017) Optimization for airgap flux density waveform of flywheel motor using NSGA-2 and Kriging model based on MaxPro Design. IEEE Trans Magn 53(8):1–7
37. Sun X, Shi Z, Zhu J (2021) Multiobjective design optimization of an IPMSM for EVs based on fuzzy method and sequential taguchi method. IEEE Trans Ind Electron 68(11):10592–10600
38. Shi Z, Sun X, Cai Y, Yang Z (2020) Robust design optimization of a five-phase PM hub motor for fault-tolerant operation based on taguchi method. IEEE Trans Energy Convers 35(4):2036–2044
39. Sun X, Shi Z, Lei G, Guo Y, Zhu J (2021) Multi-objective design optimization of an IPMSM based on multilevel strategy. IEEE Trans Ind Electron 68(1):139–148

Publisher's Note Springer Nature remains neutral with regard to jurisdictional claims in published maps and institutional affiliations.